



Cite this: *Nanoscale*, 2019, **11**, 12220

Gold nanorods functionalized by a glutathione response near-infrared fluorescent probe as a promising nanoplatform for fluorescence imaging guided precision therapy†

Yan Huang,^a Qingluan Liu,^b Yunqing Wang,^{*a} Na He,^a Rongfang Zhao,^a Jaebum Choo[†]  ^{*c} and Lingxin Chen[†]  ^{*a,d,e,f}

Theranostics nanoplatforms offer opportunities for imaging-guided precision therapy and hold great potential for clinical applications. In most reported works, the imaging unit has a lack of site selectivity, and is always kept in the “on” modality regardless of whether it is in normal tissues or tumor sites, increasing the risk of unsafe treatment. Herein, we designed a near-infrared (NIR) fluorescence-guided theranostics nanoplatform by integrating the functions of tumor-response and photodynamic therapy (PDT)/ photothermal therapy (PTT). A novel NIR fluorescent dye, CyPT, with excellent optical and PDT/PTT properties, was synthesized and linked onto the gold nanorods (AuNRs) to form CyPT–AuNRs nanohybrids via a sulfur–sulfur bond that can be broken by glutathione (GSH) with high selectivity and sensitivity. In normal cells where the concentration of GSH is low, the fluorescence of CyPT is quenched by the AuNRs. By contrast, the high level of GSH in tumor cells leads to the breaking of the sulfur–sulfur bond, resulting in the release of CyPT and the accomplishment of a “off–on” fluorescence response. Followed by precise NIR tumor-imaging diagnosis, the PDT and PTT treatment which rely on the released CyPT and AuNRs, respectively, can be effectively performed. The CyPT–AuNRs nanoplatform has been successfully applied to the treatment of tumor xenograft models and no distinct damage has been observed in the nearby normal tissues. This versatile nanoplatform has potential for use in targeted tumor imaging and precision therapy.

Received 16th March 2019,

Accepted 3rd June 2019

DOI: 10.1039/c9nr02296a

rsc.li/nanoscale

1. Introduction

Theranostics nanoplatforms integrate both diagnostic and treatment functions into a single nanoparticle, and have a

great potential to achieve imaging-guided precision therapy.^{1–4} Until now, significant efforts have been made to integrate multiple imaging probes, including fluorescence, ultrasound, magnetic resonance, X-ray-computed tomography and photoacoustic imaging, with therapeutic agents to realize this goal.^{5–10} In most theranostics nanoplatforms, these two functional units are simply combined and the imaging signal *in vivo* has a lack of site selectivity, which is always kept in the “on” modality regardless of whether it is in normal tissues or tumor sites. This causes a poor signal-to-noise ratio, obvious side effects and ‘false positive’ diagnosis results in healthy tissues and organs during the following treatment process. To increase the safety of theranostics nanoplatforms, tumor selective, activatable imaging-guided therapeutic agents have been developed in recent years. The design strategy means that the signal only appears in the accurate site by activating the imaging unit and then activating the therapeutic effect by physical stimulus-responsive (light, magnetic field, X-ray, radiofrequency, ultra-sound)^{11–15} or endogenous chemical species (some small molecule, protein, receptor and enzyme).^{16–21} The therapy allows spatial and time control of the treatment

^aCAS Key Laboratory of Coastal Environmental Processes and Ecological Remediation, The Research Center for Coastal Environmental Engineering and Technology, Yantai Institute of Coastal Zone Research, Chinese Academy of Sciences, Yantai 264003, China. E-mail: yqwang@yic.ac.cn, lxchen@yic.ac.cn

^bThe Third Division of Clinical Medicine, China Medical University, Shenyang 110122, China

^cDepartment of Chemistry, Chung-Ang University, Seoul 06974, South Korea. E-mail: jbchoo@cau.ac.kr

^dLaboratory for Marine Biology and Biotechnology, Pilot National Laboratory for Marine Science and Technology, Qingdao 266237, China

^eInstitute of Anticancer Agents Development and Theranostic Application, The Key Laboratory of Life-Organic Analysis and Key Laboratory of Pharmaceutical Intermediates and Analysis of Natural Medicine, Department of Chemistry and Chemical Engineering, Qufu Normal University, Qufu, 273165, China

^fCenter for Ocean Mega-Science, Chinese Academy of Sciences, Qingdao 266071, China

†Electronic supplementary information (ESI) available. See DOI: 10.1039/c9nr02296a

only within the site of interest. Therefore, tumor targeting precision imaging is essential for therapy to guide activation at the accurate site. The application of photodynamic therapy (PDT) and photothermal therapy (PTT) are becoming more and more widespread owing to their high spatial resolution, low toxicity, minimal side effects and tumor targeting abilities.¹² However, previous PDT and PTT treatment in tumors involved almost no activation studies. Hence, the design of a nanoplatform with a diagnostic and treatment function and activation of the PDT and PTT only within tumor site, thereby avoiding damage to normal tissues and organs, is still necessary.

It has been reported that the glutathione (GSH) level in tumor cells is much higher than in normal cells,^{22–26} because GSH plays a distinct role in tumor resistance, metastasis and angiogenesis and also influences multiple signaling pathways in the tumor microenvironment. The tumor cells have higher concentrations of GSH levels compared to normal cells.²² Thus, GSH can be considered as an endogenous factor which can be used to distinguish normal cells and tumor cells.^{22,24–26} This feature enables the development of a GSH-responsive ‘off-on’ fluorescent nanoprobe, which turns on only at the site of tumor tissue. Typically, the disulfide bond (–S–S–) has been the most popular response unit to design a GSH-responsive system,^{27–30} as it can be specifically broken by GSH, avoiding interference from other *in vivo* reactive sulfur species. Therefore, establishing an ideal and simple fluorescence nanoplatform integrating both the detection of GSH and PDT/PTT in tumors is necessary and feasible.

More importantly, apoptosis often occurs in mitochondria.^{31–33} Therefore, a photosensitizer that has a targeting function for mitochondria would have outstanding ability for PDT and PTT treatment. The design of distinctive photosensitizers has been reported which have the function of mitochondrial-targeting owing to its positive charge structure.^{34,35} Recently, gold nanorods (AuNRs) caused widespread interest owing to their excellent photophysical properties, biocompatibility, low toxicity and absorption in the near-infrared (NIR) range.^{36,37} Optical imaging and phototherapy with NIR (650–900 nm) fluorophores shows high sensitivity and deep tissue penetration because of the low tissue autofluorescence and absorption.^{38,39} Simultaneously, the nanoscale of the AuNRs mean that they can obviously accumulate in the tumor site *via* the enhanced permeability and retention effect (EPR effect) without a tumor-targeting ligand.^{40,41} Although the clearance of AuNRs was unsatisfactory compared to small gold nanoclusters,⁴² AuNRs have been applied for the targeted diagnosis of tumors and in drug delivery for tumors.^{43,44} More importantly, AuNRs play the role of both the PTT reagent and an ultra-efficient quencher owing to the photothermal conversion efficiency and obvious NIR absorption, the majority of photosensitizers with NIR emission can be quenched using AuNRs.^{18,45} This provides the opportunity to design an “off-on” activatable theranostic nanoprobe for imaging and synergistic PDT and PTT at the site of the tumor.

In this report, we developed a nanoprobe for the detection of GSH and synergistic PDT and PTT of the tumor. Firstly, the

heptamethine cyanine dye (CyPT) was synthesized as an efficient photosensitizer, which has a mitochondrial-targeting function owing to the positive charge structure. Then, AuNRs and CyPT were connected using a disulfide bond as the linker. The fluorescence of CyPT is quenched by the Förster resonance energy transfer (FRET) between the CyPT and AuNRs. The disulfide bond can be specifically broken with GSH and can then release free CyPT to “turn on” the fluorescence for PDT and PTT. The released CyPT are able to target the mitochondria owing to their positive charge structure. The CyPT–AuNRs display a high selectivity and sensitivity towards GSH *in vitro* and *in vivo*. Moreover, the nanoplatform can be used for the detection of GSH in tumor-bearing mice without interference from background fluorescence owing to the NIR fluorescence emission. CyPT–AuNRs can also accumulate in tumor tissue owing to the EPR effect. Overall, our nanoplatform not only demonstrates specific tumor-targeted imaging, but also exhibits an efficient PDT and PTT effect, and holds great promise for use in the field of tumor treatment.

2. Experimental

The list of instruments, materials, synthetic methods, results of the chemical analysis and flow cytometry are listed in the ESI.†

2.1 Cell staining procedures and colocalization-imaging experiments

The cells were plated on 6-well plates and allowed to adhere at 37 °C and 5% CO₂ for 24 h before imaging. The culture medium was then removed, and the cells were washed once with 1 mL of Dulbecco's modified eagle medium (DMEM). A549 cells were placed in 1 mL of DMEM and loaded with 60 μg mL⁻¹ CyPT–AuNRs for 3 h, before washing the cells three times with DMEM to remove the excess CyPT–AuNRs. Finally, 1 μg mL⁻¹ of mitochondrial tracker (MitoTracker Green FM, Thermo Fisher Scientific Inc.) was added and the cells were incubated for another 10 min at 37 °C. Finally, the cells were rinsed with DMEM three times and mounted on the microscope. Fluorescent images were acquired on an Olympus Fluo View FV1000 confocal laser-scanning microscope (Japan) with an objective lens (×60). The spectrally separated images acquired from the three dyes were estimated using Image-Pro Plus software.

2.2 Establishing A549 tumor xenografts models

Athymic nude mice (aged 5–6 weeks, weighing 20–25 g) were purchased from Binzhou Medical University. For the A549 tumor xenografts, 5 × 10⁶ A549 cancer cells suspended in 200 μL PBS were subcutaneously implanted into the right flank of each athymic nude mouse. All animals were maintained under aseptic conditions and were housed in groups of five in standard cages with free access to food and water and a 12 h light/dark cycle. The tumors were allowed to grow for about 8–10 days until the tumor diameter reached 8–10 mm.

2.3 *In vivo* tumor NIR fluorescent imaging and thermal imaging

The animals with A549 tumor xenograft models were used for tumor-targeted NIR imaging, after being intravenously injected with $60 \mu\text{g mL}^{-1}$ CyPT–AuNRs, with the PerkinElmer IVIS Lumina XRMS Series III *In Vivo* Imaging System. NIR imaging of the entire animal *in vivo* was performed at different times (0.5, 6, 24, 48 and 72 h) post drug injection. After sacrifice of the mice at 0.5, 6, 24, 48 and 72 h, the major organs and tumors were dissected for *ex vivo* NIR fluorescent imaging, and for studying of their tissue distribution. For the *in vivo* assessment of the PTT properties, mice with A549 tumor xenografts were intravenously injected with CyPT–AuNRs ($60 \mu\text{g mL}^{-1}$). After injection, the real-time temperature change of the mice was imaged using an infrared thermal camera (Testo 865, Germany) after the entire tumor tissue was exposed to a continuous NIR laser beam (808 nm, 1.5 W cm^{-2} , 0–5 min). Prior to NIR fluorescence or thermal imaging, mice were anesthetized by the inhalation of isoflurane.

2.4 Ethical statement

All experimental procedures were conducted in conformity with institutional guidelines for the care and use of laboratory animals, and protocols were approved by the Institutional Animal Care and Use Committee in Binzhou Medical University, Yantai, China. Approval number: no. BZ2014-102R.

3. Results and discussion

3.1 Synthesis and characterization of CyPT–AuNRs

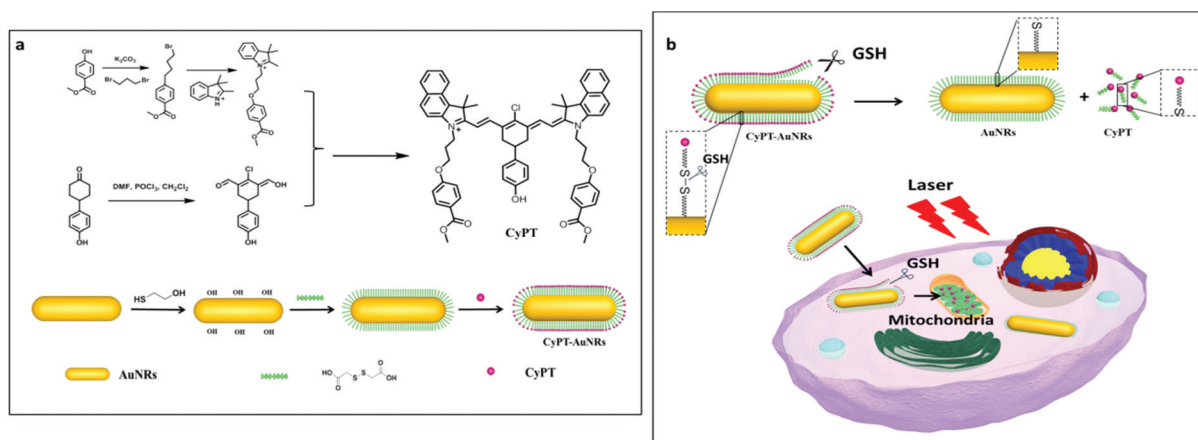
The design and application of CyPT–AuNRs is illustrated in Scheme 1a. The AuNRs were prepared according to Wang *et al.*⁴⁵ with a small modification, the CyPT was synthesized and the synthetic approaches are outlined in the ESI.† 2-Mercaptoethanol modified AuNRs were reacted with thiodiglycolic acid (for the introduction of the –S–S– bond) *via*

an esterification reaction (yield: 57%). Then, CyPT was linked to AuNRs through the terminal-hydroxyl group and the free carboxyl group of the thiodiglycolic acid on AuNRs (yield: 42%). The activatable behavior is illustrated in Scheme 1b. When the nanoplatform is in a tumor environment, the –S–S– bond can be cleaved by the high level of GSH, the free CyPT not only emits NIR fluorescence to indicate the precise location of the tumor and the accurate concentration of GSH can be determined through *in vivo* deep tissue imaging, but the mitochondria of the tumor cells can also be targeted for effective PDT therapy, together with the PTT effect from the free AuNRs upon NIR laser irradiation.

We then characterized the prepared CyPT–AuNRs using transmission electron microscopy (TEM), ultraviolet-vis-near-infrared absorption (UV-vis-NIR) and fluorescence spectroscopy. The structure of CyPT was characterized using ¹H NMR, ¹³C NMR, and high-resolution mass spectrometry (HRMS), as described in the ESI.† The as-prepared CyPT–AuNRs are well-dispersed in water. The TEM image revealed that the CyPT–AuNRs are monodispersed and have dimensions of $(48.5 \pm 2.2) \times (10.7 \pm 1.1) \text{ nm}$ (Fig. 1a). The absorption wavelength of the AuNRs was determined using these dimensions.

To determine the concentration of CyPT bound to the surface of the AuNRs, UV-vis titration of CyPT was carried out at pH 7.4 (Fig. S1†). Then, a solution of CyPT–AuNRs at $60 \mu\text{g mL}^{-1}$ was treated with DTT (20 mM) and NaCl (4 M) for 30 min (the strong binding ability of DTT to AuNRs makes CyPT depart from the AuNRs,^{18,46,47} and the resulting mixture was then centrifuged. The supernatant was collected and its absorbance at 830 nm was measured using UV-vis-NIR spectroscopy. The concentration of the CyPT in the supernatant was determined using a standard calibration method. The UV-vis-NIR titration revealed that about $6 \mu\text{M}$ CyPT was equivalent to a concentration of $60 \mu\text{g mL}^{-1}$ CyPT–AuNRs.

The spectroscopic properties of the nanoprobe were studied in buffer solution (10 mM HEPES pH 7.4). As shown as Fig. 1b,



Scheme 1 (a) The synthesis of CyPT and the CyPT–AuNRs. (b) The mechanism of the CyPT–AuNRs for the detection of GSH and the PDT/PTT of tumors.

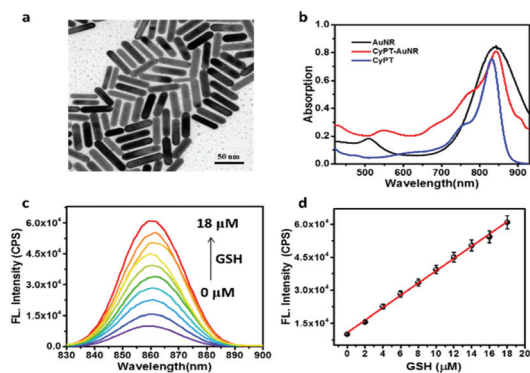


Fig. 1 (a) A representative TEM image for CyPT–AuNRs. (b) Absorption spectra of CyPT, AuNRs and CyPT–AuNRs. (c) Fluorescence emission spectra of CyPT–AuNRs and different added concentrations of GSH (0–18 μM). (d) Fluorescence emission spectra changes of CyPT–AuNRs in the presence of various concentrations of GSH. All data were acquired in HEPES (pH 7.4, 10 mM) at 37 $^{\circ}\text{C}$ ($\lambda_{\text{ex}} = 810 \text{ nm}$, $\lambda_{\text{em}} = 830\text{--}900 \text{ nm}$).

the band at 843 nm originated from the longitudinal absorption of the AuNRs. CyPT has two bands at 750 and 830 nm. This is a benefit for the occurrence of FRET between CyPT and the AuNRs owing to the band coverage at 830 nm. For the CyPT–AuNRs two characteristic absorption bands appear indicating the formation of the nanohybrid. One absorption band appears at 843 nm and its intensity and position showed no obvious change in comparison with the AuNRs, indicating that no detectable aggregation has occurred.^{48–50} The above results also indicate that the conjugation of CyPT and AuNRs did not affect the inherent absorption properties of the AuNRs. The activatable behavior was verified using fluorescence titration by the addition of GSH to the CyPT–AuNRs solution. As shown in Fig. 1c, the fluorescence emission intensity of the CyPT–AuNRs apparently enhanced with a maximum at 860 nm owing to the release of CyPT. Both the absorption and fluorescence emission maximum are located in the NIR region. As shown as Fig. 1d, the calibration curve for the CyPT–AuNRs was constructed, and a good linearity was obtained with a concentration of GSH ranging from 0 to 18 μM . The regression equation was $F_{860 \text{ nm}} = 2.80 \times 10^3 [\text{GSH}] (\mu\text{M}) + 1.08 \times 10^4$ ($r = 0.9982$). A quenching constant (K_{sv}) of $2.805 \times 10^5 \text{ L mol}^{-1}$ was obtained using the Stern–Volmer equation. The detection limit ($S/N = 3$) toward GSH was calculated to be 0.1 μM , suggesting that the CyPT–AuNRs are highly sensitive to GSH. These results indicated that the CyPT–AuNRs has good fluorescent properties, which makes them a promising candidate for application in cells.

3.2 Cell imaging of GSH and organelle localization

Encouraged by the sensitive and selective detection of GSH by the CyPT–AuNR nanoprobe, we tried to exploit the potential application of GSH detection in cells and *in vivo*. Therefore, we investigated the ability of CyPT–AuNRs for GSH detection in living cells. Initially, human lung cancer cell lines (A549 cells) were incubated with 60 $\mu\text{g mL}^{-1}$ CyPT–AuNRs for 3 h at 37 $^{\circ}\text{C}$.

Then, the cells were washed three times with DMEM to remove the excess CyPT–AuNRs. The cells showed almost no fluorescence in the control, as seen in Fig. 2a. However, after incubation with 100 μM GSH, the cells displayed apparent levels of fluorescence in the cells, the fluorescence signal became stronger and stronger and rose to a plateau within 30 min. These results demonstrated that the nanoprobe CyPT–AuNRs were suitable for the detection of exogenous GSH.

Furthermore, the endogenous GSH in living cells was detected using CyPT–AuNRs. Human normal lung fibroblast cells lines (MRC-5 cells) (normal cells) and A549 cells (tumor cells) were selected as the cell models. Firstly, we used a Total Glutathione Assay Kit to detect the GSH levels in A549 cells and MRC-5 cells, the results indicated that the GSH concentration in A549 cells was about 2.4-fold higher than the MRC-5 cells (Fig. S6[†]). Then, the endogenous GSH content in normal cells and tumor cells was detected using the CyPT–AuNRs, respectively. All of the tested cells were incubated with 60 $\mu\text{g mL}^{-1}$ CyPT–AuNRs at 37 $^{\circ}\text{C}$ before imaging. In addition, we regulated the laser power of the laser scanning confocal microscope to use the fluorescence intensity of the MRC-5 cells as a control. As shown in Fig. 2b, the fluorescence signal in the A549 cells was much higher than the MRC-5 cells after 3 h. To verify whether the A549 cells ingested more CyPT–AuNRs than the MRC-5 cells, we tried to detect the content of CyPT–AuNRs in A549 cells and MRC-5 cells using inductively coupled plasma mass spectrometry (ICP-MS). The mass of the gold element in the A549 cells and MRC-5 cells was determined from the ICP-MS analysis. The results indicated that the content of CyPT–AuNRs in the A549 cells was 1.5-fold higher than in the MRC-5 cells (Fig. S7[†]). These results all indicated that the fluorescence signal in the A549 cells was much higher than the MRC-5 cells, which was attributed to both the higher concentrations of GSH levels in the tumor cells and the greater amount of CyPT–AuNRs ingested by the tumor cells. Overall, the results suggested that CyPT–AuNRs have great potential and are suitable for PDT and PTT treatment in tumor cells. Then, *N*-ethylmaleimide (NEM) was employed as a scavenger for GSH and lipopolysaccharide (LPS) was employed as an accelerator for GSH. A549 cells were treated with 5 mM NEM for 30 min in order to consume all of the GSH,⁵¹ then, the cells were treated with 60 $\mu\text{g mL}^{-1}$ CyPT–AuNRs, until almost no fluorescence signal was observed in the cells (Fig. 2c). It is reported that LPS can induce cystathionine γ -lyase (CSE) mRNA overexpression in A549 cells for promoting the initial real-time production rate of RSH.⁵² Another group of cells were stimulated with 1 $\mu\text{g mL}^{-1}$ LPS for 30 min. Then, the cells were treated with 60 $\mu\text{g mL}^{-1}$ CyPT–AuNRs. As shown in Fig. 2c, we observed an obvious fluorescence enhancement. This indicated that the free CyPT was released from the CyPT–AuNRs owing to the stimulation of GSH. All of the fluorescence responses were additionally verified using a flow cytometry assay owing to its statistically reliable data analysis (Fig. 2a–c).⁵³ The above described results suggest that the CyPT–AuNRs demonstrate a strong fluorescence enhancement *via* the stimulation of exogenous or endogenous GSH in living cells.

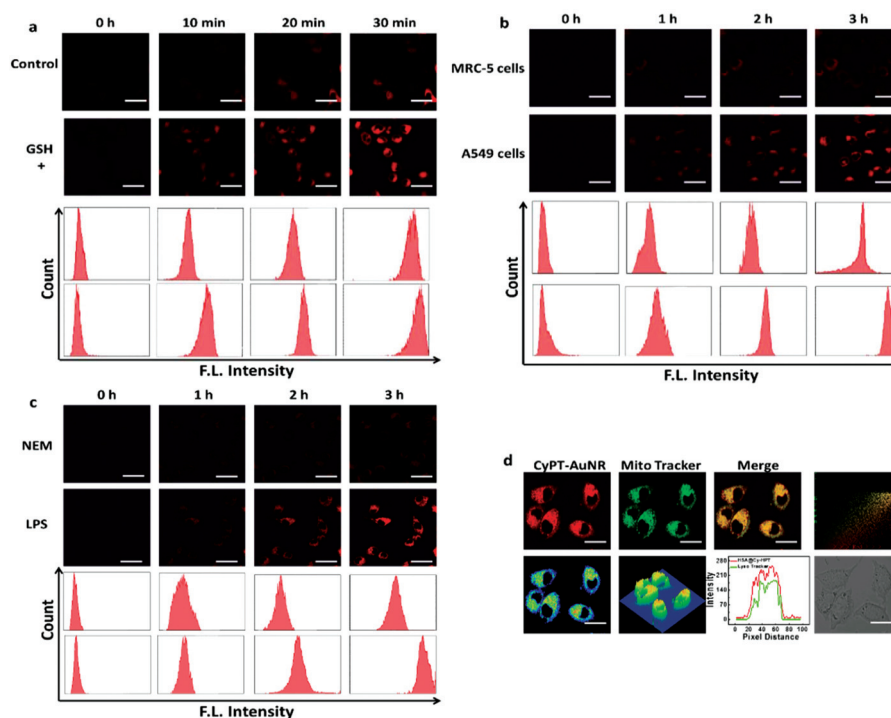


Fig. 2 (a) The detection of exogenous GSH using CyPT-AuNRs in A549 cells using a laser scanning confocal microscope. (b) The endogenous GSH content in normal cells (MRC-5 cells) and tumor cells (A549 cells) were detected using CyPT-AuNRs at different time periods. (c) A549 cells treated with CyPT-AuNRs for the detection of endogenous GSH in different time periods (scale bar: 40 μm). (d) Mitochondrial localization of CyPT-AuNRs was carried out by co-localization of CyPT-AuNRs and the Mito Tracker in A549 cells (red channel: $\lambda_{\text{ex}} = 810 \text{ nm}$, $\lambda_{\text{em}} = 830\text{--}900 \text{ nm}$). MitoTracker Green FM showing mitochondria (green channel: $\lambda_{\text{ex}} = 488 \text{ nm}$, $\lambda_{\text{em}} = 500\text{--}580 \text{ nm}$). Images are representative of $n = 5$ independent experiments. Scale bar: 10 μm .

In order to examine the organelle-targeting ability and the method of cell internalization of the CyPT-AuNRs, a colocalization experiment was carried out. As we know, apoptosis often occurs in mitochondria.^{31–33} Therefore, a photosensitizer that has a mitochondrial-targeting function would give effective PDT and PTT. Therefore, we verified whether the released CyPT had a mitochondrial-targeting function. After the A549 cells were incubated with CyPT-AuNRs ($60 \mu\text{g mL}^{-1}$) for 3 h, the mitochondrial localization of the released CyPT was confirmed in living cells (Fig. 2d) using a mitochondrial tracker (MitoTracker Green FM) ($1 \mu\text{g mL}^{-1}$). We observed that the red fluorescence of the released CyPT precisely coincided with the green fluorescence of the mitochondrial tracker. The Manders' coefficients $m_1 = 0.97$, $m_2 = 0.95$ and the Pearson's coefficient $R_r = 0.94$ suggested that the released CyPT was preferentially distributed in the mitochondria (Fig. 2d). These imaging results suggested that the released CyPT from the CyPT-AuNRs could accumulate exclusively in the mitochondria of cancer cells owing to its positive charge structure.

3.3 Evaluation of singlet oxygen generation efficiency and photothermal conversion of CyPT-AuNRs

Next, we further verified whether the CyPT-AuNRs had a PDT/PTT effect after detection of GSH. The singlet oxygen signals ($^1\text{O}_2$) generated from the CyPT-AuNRs exposed to an 808 nm NIR laser at 1.5 W cm^{-2} in the presence or absence of GSH

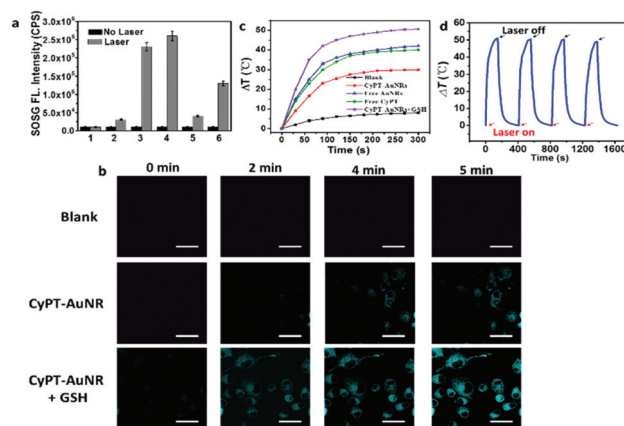


Fig. 3 (a) The fluorescence data for the singlet oxygen probe (SOSG): 1. Blank; 2. CyPT-AuNRs; 3. CyPT-AuNRs + GSH; 4. free CyPT; 5. free AuNRs; 6. ICG. (b) Fluorescent images of A549 cells at different time periods for analysis of the generated $^1\text{O}_2$ using SOSG. Fluorescence channel: $\lambda_{\text{ex}} = 490 \text{ nm}$, $\lambda_{\text{em}} = 510\text{--}560 \text{ nm}$. Scale bar = 40 μm . (c) Temperature curves for the CyPT-AuNRs, CyPT-AuNRs + GSH, free CyPT and free AuNRs under 808 nm laser irradiation for 5 min. (d) Evaluation of the photothermal stability of CyPT-AuNRs with an 808 nm continuous laser and switching the laser off for four cycles.

were also compared by using the singlet oxygen sensor green (SOSG, Invitrogen co., USA) as a probe. As shown as Fig. 3a, comparison of the CyPT-AuNRs, CyPT-AuNRs + GSH, free

CyPT (equivalent concentrations of CyPT–AuNRs) and free AuNRs (equivalent concentrations of CyPT–AuNRs), CyPT–AuNRs and free AuNRs revealed almost no fluorescence signal for SOSG, and the CyPT–AuNRs + GSH and free CyPT displayed a strong fluorescence signal for SOSG using the fluorescence spectrometer. The fluorescence emission spectra of SOSG indicated that $^1\text{O}_2$ was generated *via* CyPT in the solution. However, the $^1\text{O}_2$ production of CyPT–AuNRs + GSH was less than that of the free CyPT. This might mean that the reaction of CyPT–AuNRs and GSH was incomplete. The $^1\text{O}_2$ generation *via* CyPT–AuNRs + GSH and a clinically available heptamethine cyanine dye indocyanine green (ICG) were compared.⁵⁴ Results indicated that CyPT–AuNRs + GSH exhibited greater $^1\text{O}_2$ generation than that of ICG (Fig. 3a). Next, the $^1\text{O}_2$ generation of CyPT–AuNRs in living cells under NIR laser irradiation was studied. SOSG was used to detect the generated $^1\text{O}_2$ by cells fluorescence imaging. First, a group of A549 cells were used as the control, two groups of cells were treated with $60\ \mu\text{g mL}^{-1}$ CyPT–AuNRs for 3 h at $37\ ^\circ\text{C}$, then, one group of cells were additional treated with $100\ \mu\text{M}$ GSH for 30 min. All cells were treated with $1\ \mu\text{M}$ SOSG. All of the cells were exposed to a NIR laser (808 nm) at $1.5\ \text{W cm}^{-2}$ for 0, 2, 4 and 5 min, respectively, and fluorescence images were obtained. As shown in Fig. 3b, the blank group and the CyPT–AuNR group showed a weak fluorescence and the CyPT–AuNRs + GSH group emitted a strong fluorescence. These imaging analyses provided evidence that the CyPT–AuNRs could generate $^1\text{O}_2$ in the presence of GSH in living cells under laser irradiation. According to the above-mentioned studies, the CyPT–AuNRs are potential multifunctional nanoparticles for PDT/PTT therapy.

In view of the excellent photoconverted thermal ability of the single CyPT and single AuNRs, and the remarkable photodynamic properties of the CyPT–AuNR nanoparticles, next we analyzed the photoconverted thermal effect of the CyPT–AuNRs. Four groups were chosen as the test subjects, a CyPT–AuNR group, CyPT–AuNRs + GSH group, free CyPT group and a free AuNR group. As expected, compared with the single

CyPT–AuNRs, the solution of free CyPT and free AuNRs exhibited an obvious temperature increase upon 808 nm NIR laser irradiation at $1.5\ \text{W cm}^{-2}$ for 5 min (Fig. 3c). We hypothesized that the FRET between the CyPT and AuNRs in the CyPT–AuNRs weakened the photoconverted thermal effect compared with the free CyPT and free AuNRs. Interestingly, the temperature rise observed for the CyPT–AuNRs + GSH group was higher than the free CyPT and free AuNRs. We reasoned that the synergetic effect of the CyPT and AuNRs in the CyPT–AuNRs + GSH solution had a superior photoconverted thermal effect. The temperature of the CyPT–AuNRs + GSH solution at a concentration of $60\ \mu\text{g mL}^{-1}$ rose rapidly over $50\ ^\circ\text{C}$ within 5 min. The photothermal conversion efficiency of the CyPT–AuNRs + GSH were quantitatively measured and calculated to be 48.39%. Evaluation of the photothermal performance of the nanoprobe indicated that it could speedily and efficiently convert photoenergy into heat. To verify the circulation heating ability of the CyPT–AuNRs + GSH, the photothermal stability of the CyPT–AuNRs + GSH was also measured by irradiating the sample with an 808 nm continuous laser and turning off the laser for four cycles. As shown in Fig. 3d, we found that the temperature changes showed no obvious reduction. All of these results indicated that the –S–S– of the CyPT–AuNRs could be interrupted by the GSH, and that CyPT was released and led to restoration of its fluorescence, thus the CyPT–AuNRs demonstrate effective PDT/PTT therapy as multifunctional nanoparticles.

3.4 Cytotoxicity assay and photoinduced cytotoxicity

The cytotoxicity of the nanoprobe is the key factor used to evaluate whether it can be applied in clinical applications. First, we performed a standard MTT assay to evaluate the cytotoxicity nonirradiation of the CyPT–AuNRs, free CyPT (equivalent concentrations of CyPT–AuNRs) and free AuNRs. As demonstrated in Fig. 4a, more than 85% of the A549 cells survived after the cells were incubated with $100\ \mu\text{g mL}^{-1}$ CyPT–AuNRs for 24 h. However, free AuNRs exhibited an obvious

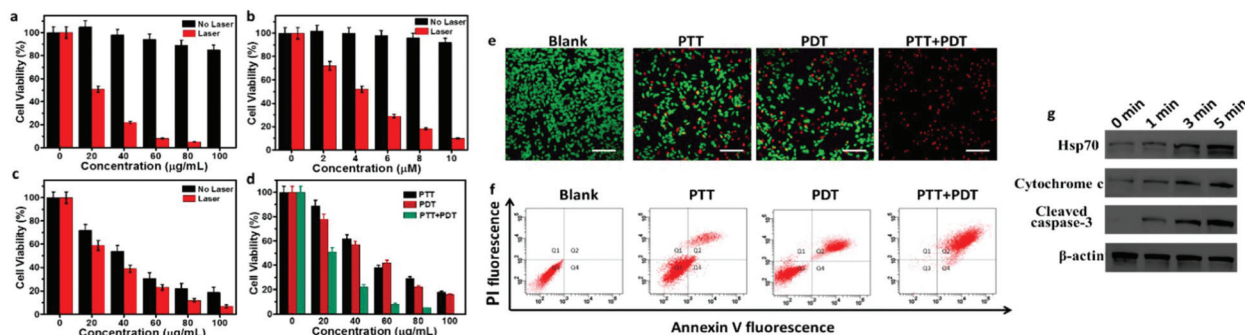


Fig. 4 MTT assay for the cytotoxicity of: (a) CyPT–AuNRs; (b) free CyPT; and (c) free AuNRs for A549 cells upon laser irradiation or no laser irradiation. (d) Cell viability under synergetic PDT and PTT, single PTT or single PDT of CyPT–AuNRs for A549 cells with laser irradiation. (e) Calcein AM/PI co-stained imaging of A549 cells after synergetic PDT and PTT, single PTT or single PDT after treatment with CyPT–AuNRs using a laser scanning confocal microscope. Scale bar = $200\ \mu\text{m}$. (f) Apoptosis analysis of Annexin V-PE under blank, synergetic PDT and PTT, single PTT or single PDT using flow cytometry. (g) Protein expression of Hsp70, cytochrome c and cleaved caspase-3 with different laser irradiation times using western blot analysis and using the expression of β -actin as a control.

cytotoxicity, this was consistent with the previous studies.⁵⁵ The cytotoxicity of free CyPT without the application of the laser was also suitable for application in living cells and *in vivo*. For the CyPT–AuNRs the IC_{50} was found to be $345 \mu\text{g mL}^{-1}$, which indicated that the lower cytotoxicity of the CyPT–AuNRs was attributed to the positively charged molecule of CyPT on the surface of the AuNRs.⁵⁵

Next, we further verified whether the CyPT–AuNRs have the potential to demonstrate a phototherapeutic effect in complex biological systems. We evaluated the anti-cancer cell effect of the CyPT–AuNRs using PDT and PTT *in vitro*. A549 cells were cultured under recommended conditions and were incubated with CyPT–AuNRs. The MTT assay indicated that the cell viability in the laser groups decreased as the concentration of CyPT–AuNRs ($0\text{--}100 \mu\text{g mL}^{-1}$) increased, and almost no cell viability was visible at $100 \mu\text{g mL}^{-1}$ (Fig. 4a). In comparison, the cell viability in the no laser groups was almost unchanged. The free CyPT and free AuNRs exhibited a limited PTT and PDT effect. All of these data enabled the CyPT–AuNRs to demonstrate an outstanding PTT and PDT effect for anti-cancer cells.

To verify that the therapeutic effect of the CyPT–AuNRs was contributed to by synergetic PDT and PTT treatments, the single PDT and single PTT were studied, respectively.⁵⁶ When treated with CyPT–AuNRs at $100 \mu\text{g mL}^{-1}$ the MTT assay showed a 20.4% cell viability for the PTT treatment alone, and a 18.5% cell viability for PDT treatment alone, synergistic PDT and PTT treatment showed the survival of almost no cells (Fig. 4d). The results indicated that the photo-induced cytotoxicity of CyPT–AuNRs is synergistically enhanced by PDT and PTT treatment.

The effect of PDT and PTT of CyPT–AuNRs was also visibly verified using co-stained fluorescence imaging of propidium iodide (PI) and Calcein AM in A549 cells (Fig. 4e). The apoptosis rate was also evaluated using flow cytometry with an apoptosis kit (Annexin V-PE) (Fig. 4f). The cells were incubated with $100 \mu\text{g mL}^{-1}$ CyPT–AuNRs for 6 h and underwent laser irradiation for 5 min (808 nm , 1.5 W cm^{-2}). The apoptosis rate from the synergistic effect of the PDT and PTT was much higher than for the single PTT or single PDT. In addition, the cell death was mediated by the apoptosis pathways in an irradiation time-dependent manner. The heat shock protein 70 (Hsp70) is typically synthesized in response to heat stress to protect the cell from thermal or oxidative stress.⁵⁷ Therefore, the expression of Hsp70 was tested. As shown as Fig. 4g, the expression of Hsp70 was obviously overexpressed as the irradiation (808 nm , 1.5 W cm^{-2}) time increased. Western blot analysis showed that expression of the mitochondria-mediated apoptosis related proteins, such as cleaved caspase-3 and cytochrome c, was increased as the irradiation time increased (Fig. 4g), all of these results suggest that the intrinsic signal pathway regulates the cell apoptosis.

3.5 Infrared thermal imaging and anti-tumor therapy in tumor-bearing mice

In view of the outstanding photothermal conversion rate and singlet oxygen yield of the CyPT–AuNRs and the appropriate

accumulated time in the tumor site (Fig. S9[†]), the CyPT–AuNRs were used for the treatment of a tumor. A549 tumor xenograft models were employed as the test models. The tumor xenograft models were randomly grouped into four groups: models injected with PBS buffer solution without laser irradiation as the PBS nonirradiation group; the same treatment as the PBS nonirradiation group but with 808 nm NIR laser irradiation (1.5 W cm^{-2}) for 5 min was used for the PBS irradiation group; injection of CyPT–AuNRs (5 mg kg^{-1}) into the tumor xenograft models without laser irradiation was used for the CyPT–AuNRs nonirradiation group; and the same treatment as the CyPT–AuNRs nonirradiation group but with 808 nm NIR laser irradiation (1.5 W cm^{-2}) for 5 min was used for the CyPT–AuNRs irradiation group. All injections were intravenous. Thermal images were then obtained *via* a TESTO 865 Infrared Thermal Camera for real-time measurement of the temperature of the tumors. As shown in Fig. 5a, the temperature of the PBS irradiation group increased to $45 \text{ }^\circ\text{C}$ after 5 min of irradiation owing to the laser energy transfer. As expected, the temperature of the CyPT–AuNRs irradiation group was increased to about $60 \text{ }^\circ\text{C}$, which was high enough to ablate tumors.⁵⁸ A histogram of the temperatures measured in order to quantify the increase in the temperature is shown in Fig. S11.[†] These results suggested that the CyPT–AuNRs could raise the temperature of the tumor tissue using laser irradiation. Therefore, the CyPT–AuNRs have great potential for use as a diagnostic treatment reagent for PDT/PTT therapy.

To study the effect of the CyPT–AuNRs in anti-tumor treatment, we recorded the survival rate and relative tumor volume (every 2 d after irradiation). The PBS nonirradiation group and PBS irradiation group both exhibited approximately a 10-fold increase in the relative tumor volumes, indicating that a single laser irradiation had almost no effect on the tumor growth (Fig. 5b). The CyPT–AuNRs nonirradiation group also showed a faint change in the tumor growth without laser irradiation, owing to its negligible cytotoxicity (Fig. 5b). Noticeably, the CyPT–AuNRs irradiation group showed obvious tumor inhibition without regrowth under laser irradiation (Fig. 5b). This result demonstrated that the CyPT–AuNRs provided effective PDT/PTT for tumors.

To test the anti-tumor effects of the CyPT–AuNRs, we further observed the tumor-damaging ability *via* hematoxylin & eosin (H&E) staining of the tumor tissue after treatment. The body weight was also recorded to monitor the health status of the models (Fig. 5d), suggesting the good-biocompatibility and negligible side effects of the CyPT–AuNRs. Obvious damage to the tumor tissue was demonstrated by the CyPT–AuNRs irradiation group using H&E staining (Fig. 5e), indicating an excellent efficacy. However, the PBS nonirradiation group, PBS irradiation group and CyPT–AuNRs nonirradiation group all exhibited no obvious tumor damage. More importantly, the CyPT–AuNRs also caused no distinct damage to the normal tissues such as the heart, liver, spleen, lung and kidney (Fig. 5f). Therefore, it was demonstrated that the CyPT–AuNRs could provide synergistic and efficient PDT and PTT for tumors without obvious side effects.

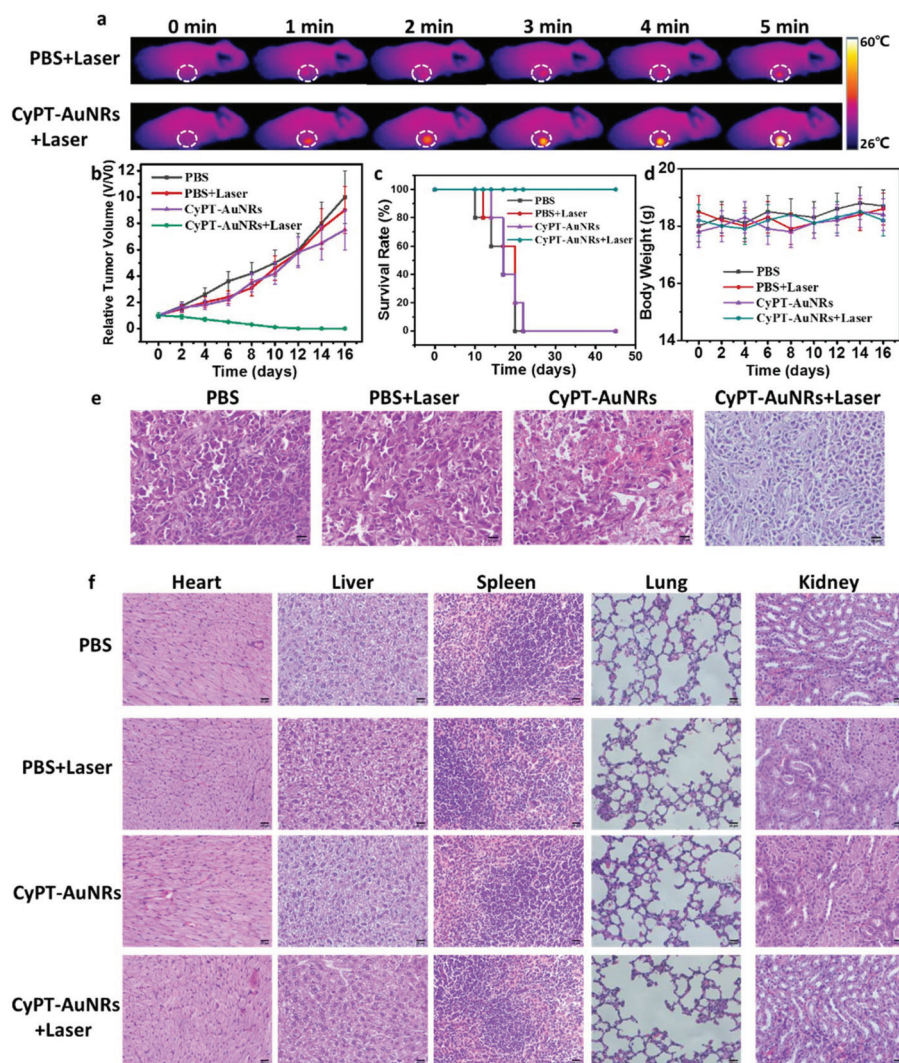


Fig. 5 (a) IR thermal images of subcutaneous A549 tumor xenograft mice during 5 min NIR laser irradiation. (b) The relative tumor volume of the subcutaneous A549 tumor xenograft mice in different groups. (c) The survival rate of A549 tumor xenograft mice in different groups. (d) The body weight of A549 tumor xenograft mice in different groups. (e) H&E staining of A549 tumor in different groups. (f) H&E staining of the normal tissues in different groups. Magnification: $\times 400$. Data are presented as mean \pm SD ($n = 5$).

4. Conclusions

In summary, we have developed a NIR fluorescent nanoprobe, CyPT-AuNRs, for the detection of GSH in living cells and *in vivo*. The CyPT-AuNRs exhibit a high selectivity and sensitivity towards GSH. In addition, the nanoprobe shows active transport into living cells by endocytosis. It was confirmed that the nanoprobe CyPT-AuNRs can be used for the detection of GSH in mice and tumor-bearing mice without interference from background fluorescence owing to its NIR fluorescence emission. Simultaneously, we have demonstrated that not only does the CyPT that is released from the CyPT-AuNRs have an excellent PDT effect *in vitro* and *in vivo*, but also that the CyPT and AuNRs both have an excellent PTT effect. Finally, the CyPT-AuNRs were successfully applied for tumor treatment in tumor-bearing mice, the results suggested that the CyPT-AuNRs could be used as tumor-targeted NIR imaging reagents *in vivo* and offer an excellent PDT/PTT

effect for the inhibition of tumor growth and could increase the survival rate. Moreover, the CyPT-AuNRs caused almost no distinct damage to the normal tissues such as the heart, liver, spleen, lung and kidney. Our strategy for the design of a theranostic nanoplatform with activatable fluorescence imaging-guided precision PDT and PTT provides a valuable approach for the construction of a smart theranostic platform for clinical applications.

Conflicts of interest

There are no conflicts to declare.

Acknowledgements

We thank the National Nature Science Foundation of China (no. 21575159, 81573393), the program of Youth Innovation

Promotion Association, CAS (grant 2017256), the Instrument Developing Project of the Chinese Academy of Sciences (YZ201662), and the National Research Foundation of Korea for supporting this work (grant numbers 2017M3D1A1039287 and 2018M3A7B4071203).

References

- M. Guan, H. Dong, J. Ge, D. Chen, L. Sun, S. Li, C. Wang, C. Yan, P. Wang and C. Shu, *NPG Asia Mater.*, 2015, **7**, e205.
- X. Chen, S. S. Gambhir and J. Cheon, *Acc. Chem. Res.*, 2011, **44**, 841.
- Y. Li, T. Y. Lin, Y. Luo, Q. Liu, W. Xiao, W. Guo, D. Lac, H. Zhang, C. Feng, S. Wachsmann-Hogiu, J. H. Walton, S. R. Cherry, D. J. Rowland, D. Kukis, C. Pan and K. S. Lam, *Nat. Commun.*, 2014, **5**, 4712.
- D. E. Lee, H. Koo, I. C. Sun, J. H. Ryu, K. Kim and I. C. Kwon, *Chem. Soc. Rev.*, 2012, **41**, 2656–2672.
- Q. Chen, J. Wen, H. Li, Y. Xu, F. Liu and S. Sun, *Biomaterials*, 2016, **106**, 144–166.
- C. Zeng, W. Shang, X. Liang, X. Liang, Q. Chen, C. Chi, Y. Du, C. Fang and J. Tian, *ACS Appl. Mater. Interfaces*, 2016, **8**, 29232–29241.
- Z. Luo, M. Zheng, P. Zhao, Z. Chen, F. Siu, P. Gong, G. Gao, Z. Sheng, C. Zheng, Y. Ma and L. Cai, *Sci. Rep.*, 2016, **6**, 23393.
- Y. Wang, T. Yang, H. Ke, A. Zhu, Y. Wang, J. Wang, J. Shen, G. Liu, C. Chen, Y. Zhao and H. Chen, *Adv. Mater.*, 2015, **27**, 3874–3882.
- Q. Xiao, X. Zheng, W. Bu, W. Ge, S. Zhang, F. Chen, H. Xing, Q. Ren, W. Fan, K. Zhao, Y. Hua and J. Shi, *J. Am. Chem. Soc.*, 2013, **135**, 13041–13048.
- J. Liu, L. Zhang, J. Lei and H. Ju, *ACS Appl. Mater. Interfaces*, 2015, **7**, 19016–19023.
- Q. Chen, H. Ke, Z. Dai and Z. Liu, *Biomaterials*, 2015, **73**, 214–230.
- L. Cheng, C. Wang, L. Feng, K. Yang and Z. Liu, *Chem. Rev.*, 2014, **114**, 10869–10939.
- G. Mikhaylov, U. Mikac, A. A. Magaeva, V. I. Itin, E. P. Naiden, I. Psakhye, L. Babes, T. Reinheckel, C. Peters, R. Zeiser, M. Bogoyo, V. Turk, S. G. Psakhye, B. Turk and O. Vasiljeva, *Nat. Nanotechnol.*, 2011, **6**, 594–602.
- A. Sasidharan, A. J. Sivaram, A. P. Retnakumari, P. Chandran, G. L. Malarvizhi, S. Nair and M. Koyakutty, *Adv. Healthcare Mater.*, 2015, **4**, 679–684.
- W. Chen and J. Du, *Sci. Rep.*, 2013, **3**, 2162.
- J. Li, F. Cheng, H. Huang, L. Li and J. J. Zhu, *Chem. Soc. Rev.*, 2015, **44**, 7855–7880.
- L. Zhang, S. Gao, F. Zhang, K. Yang, Q. Ma and L. Zhu, *ACS Nano*, 2014, **8**, 12250–12258.
- D. K. Yi, I. C. Sun, J. H. Ryu, H. Koo, C. W. Park, I. C. Youn, K. Choi, I. C. Kwon, K. Kim and C. H. Ahn, *Bioconjugate Chem.*, 2010, **21**, 2173–2177.
- N. Li, T. Li, C. Hu, X. Lei, Y. Zuo and H. Han, *ACS Appl. Mater. Interfaces*, 2016, **8**, 15013–15023.
- S. Gao, L. Zhang, G. Wang, K. Yang, M. Chen, R. Tian, Q. Ma and L. Zhu, *Biomaterials*, 2016, **79**, 36–45.
- X. Ai, C. J. Ho, J. Aw, A. B. Attia, J. Mu, Y. Wang, X. Wang, Y. Wang, X. Liu, H. Chen, M. Gao, X. Chen, E. K. Yeow, G. Liu, M. Olivo and B. Xing, *Nat. Commun.*, 2016, **7**, 10432.
- N. Traverso, R. Ricciarelli, M. Nitti, B. Marengo, A. L. Furfaro, M. A. Pronzato, U. M. Marinari and C. Domenicotti, *Oxid. Med. Cell. Longevity*, 2013, **2013**, 972913.
- E. Suess, S. Malessa, K. Ungersbock, P. Kitz, I. Podreka, K. Heimberger, O. Hornykiewicz and L. Deecke, *J. Nucl. Med.*, 1991, **32**, 1675–1681.
- A. Gupta, S. Srivastava, R. Prasad, S. M. Natsu, B. Mittal, M. P. Negi and A. N. Srivastava, *Respirology*, 2010, **15**, 349–356.
- G. Almadori, F. Bussu, J. Galli, A. Limongelli, S. Persichilli, B. Zappacosta, A. Minucci, G. Paludetti and B. Giardina, *Head Neck*, 2007, **29**, 648–654.
- P. R. Kearns, R. Pieters, M. M. Rottier, A. D. Pearson and A. G. Hall, *Blood*, 2001, **97**, 393–398.
- J. Zhu, I. Dhimitruka and D. Pei, *Org. Lett.*, 2004, **6**, 3809–3812.
- P. K. Pallela, T. Chiku, M. R. Carvan and D. S. Sem, *Anal. Biochem.*, 2006, **352**, 265–273.
- A. M. Piggott and P. Karuso, *Anal. Chem.*, 2007, **79**, 8769–8773.
- M. M. Pires and J. Chmielewski, *Org. Lett.*, 2008, **10**, 837–840.
- G. Kroemer and J. C. Reed, *Nat. Med.*, 2000, **6**, 513–519.
- D. R. Green, *Cell*, 2000, **102**, 1–4.
- T. Xiao, J. K. Fan, H. L. Huang, J. F. Gu, L. Y. Li and X. Y. Liu, *Cell Res.*, 2010, **20**, 367–378.
- S. Luo, X. Tan, S. Fang, Y. Wang, T. Liu, X. Wang, Y. Yuan, H. Sun, Q. Qi and C. Shi, *Adv. Funct. Mater.*, 2016, **26**, 2826–2835.
- X. Tan, S. Luo, L. Long, Y. Wang, D. Wang, S. Fang, Q. Ouyang, Y. Su, T. Cheng and C. Shi, *Adv. Mater.*, 2017, **29**, 1704196.
- H. C. Chang and J. A. Ho, *Anal. Chem.*, 2015, **87**, 10362–10367.
- N. Goswami, F. Lin, Y. Liu, D. T. Leong and J. Xie, *Chem. Mater.*, 2016, **28**, 4009–4016.
- J. Gao, K. Chen, R. Luong, D. M. Bouley, H. Mao, T. Qiao, S. S. Gambhir and Z. Cheng, *Nano Lett.*, 2012, **12**, 281–286.
- Q. He, Z. Zhang, F. Gao, Y. Li and J. Shi, *Small*, 2011, **7**, 271–280.
- C. Zhou, M. Long, Y. Qin, X. Sun and J. Zheng, *Angew. Chem., Int. Ed.*, 2011, **50**, 3168–3172.
- J. Liu, M. Yu, C. Zhou, S. Yang, X. Ning and J. Zheng, *J. Am. Chem. Soc.*, 2013, **135**, 4978–4981.
- B. Du, X. Jiang, A. Das, Q. Zhou, M. Yu, R. Jin and J. Zheng, *Nat. Nanotechnol.*, 2017, **12**, 1096–1102.
- H. S. Choi, W. Liu, F. Liu, K. Nasr, P. Misra, M. G. Bawendi and J. V. Frangioni, *Nat. Nanotechnol.*, 2010, **5**, 42–47.
- Z. Luo, K. Zheng and J. Xie, *Chem. Commun.*, 2014, **50**, 5143–5155.

- 45 J. H. Wang, B. Wang, Q. Liu, Q. Li, H. Huang, L. Song, T. Y. Sun, H. Wang, X. F. Yu, C. Li and P. K. Chu, *Biomaterials*, 2013, **34**, 4274–4283.
- 46 I. C. Sun, D. K. Eun, H. Koo, C. Y. Ko, H. S. Kim, D. K. Yi, K. Choi, I. C. Kwon, K. Kim and C. H. Ahn, *Angew. Chem., Int. Ed.*, 2011, **50**, 9348–9351.
- 47 S. Lee, E. J. Cha, K. Park, S. Y. Lee, J. K. Hong, I. C. Sun, S. Y. Kim, K. Choi, I. C. Kwon, K. Kim and C. H. Ahn, *Angew. Chem., Int. Ed.*, 2008, **47**, 2804–2807.
- 48 A. M. Funston, C. Novo, T. J. Davis and P. Mulvaney, *Nano Lett.*, 2009, **9**, 1651–1658.
- 49 X. Liu, N. Huang, H. Li, H. Wang, Q. Jin and J. Ji, *ACS Appl. Mater. Interfaces*, 2014, **6**, 5657–5668.
- 50 J. H. Joo and J. S. Lee, *Anal. Chem.*, 2013, **85**, 6580–6586.
- 51 X. Han, X. Song, F. Yu and L. Chen, *Chem. Sci.*, 2017, **8**, 6991–7002.
- 52 Y. Huang, F. Yu, J. Wang and L. Chen, *Anal. Chem.*, 2016, **88**, 4122–4129.
- 53 G. Horstick, T. Kempf, M. Lauterbach, M. Ossendorf, L. Kopacz, A. Heimann, H. A. Lehr, S. Bhakdi, J. Meyer and O. Kempfski, *J. Surg. Res.*, 2000, **94**, 28–34.
- 54 K. Polom, D. Murawa, Y. S. Rho, P. Nowaczyk, M. Hunerbein and P. Murawa, *Cancer*, 2011, **117**, 4812–4822.
- 55 L. Wang, X. Jiang, Y. Ji, R. Bai, Y. Zhao, X. Wu and C. Chen, *Nanoscale*, 2013, **5**, 8384–8391.
- 56 E. Friday, N. Koshy, V. K. Bhandari and F. Torturro, *Blood*, 2010, **116**, 1475.
- 57 H. Chen, A. Adam, Y. Cheng, S. Tang, J. Hartung and E. Bao, *Mol. Med. Rep.*, 2015, **11**, 2276–2284.
- 58 M. Perez-Hernandez, P. P. Del, S. G. Mitchell, M. Moros, G. Stepien, B. Pelaz, W. J. Parak, E. M. Galvez, J. Pardo and J. M. de la Fuente, *ACS Nano*, 2015, **9**, 52–61.